Structure of Self-Aggregated Alamethicin in ePC Membranes Detected by Pulsed Electron-Electron Double Resonance and Electron Spin Echo Envelope Modulation Spectroscopies

Milov, A.D.; Samoilova, R.I.; Tsvetkov, Y.D.; De Zotti, M.; Formaggio, F.; Toniolo, C.; ... ; Raap, J.

Structure of Self-Aggregated Alamethicin in ePC Membranes Detected by Pulsed Electron-Electron Double Resonance and Electron Spin Echo Envelope Modulation Spectroscopies

Alexander D. Milov,[†] Rimma I. Samoilova,[†] Yuri D. Tsvetkov,[†] Marta De Zotti,[‡] Fernando Formaggio,[‡] Claudio Toniolo,[‡] Jan-Willem Handgraaf,[§] and Jan Raap[¶*]

[†]Institute of Chemical Kinetics and Combustion, Novosibirsk, 630090 Russian Federation; [‡]Institute of Biomolecular Chemistry, CNR, Padova Unit, Department of Chemistry, University of Padova, 35131 Padova, Italy; [§]Culgi B.V., Leiden, The Netherlands; and [¶]Leiden Institute of Chemistry, Gorlaeus Laboratories, Leiden University, Leiden, The Netherlands

ABSTRACT PELDOR spectroscopy was exploited to study the self-assembled super-structure of the [Glu(OMe)^{7,18,19}]alamethicin molecules in vesicular membranes at peptide to lipid molar ratios in the range of 1:70–1:200. The peptide molecules were site-specifically labeled with TOAC electron spins. From the magnetic dipole-dipole interaction between the nitroxides of the monolabeled constituents and the PELDOR decay patterns measured at 77 K, intermolecular-distance distribution functions were obtained and the number of aggregated molecules ($n \approx 4$) was estimated. The distance distribution functions exhibit a similar maximum at 2.3 nm. In contrast to Alm16, for Alm1 and Alm8 additional maxima were recorded at 3.2 and ~5.2 nm. From ESEEM experiments and based on the membrane polarity profiles, the penetration depths of the different spin-labeled positions into the membrane were qualitatively estimated. It was found that the water accessibility of the spin-labels follows the order TOAC-1 $>$ TOAC-8 $\approx$ TOAC-16. The geometric data obtained are discussed in terms of a penknife molecular model. At least two peptide chains are aligned parallel and eight ester groups of the polar Glu(OMe)^{18,19} residues are suggested to stabilize the self-aggregate superstructure.

INTRODUCTION

Alamethicin is a peptide containing 19 amino acid residues and a 1,2-aminoalcohol (phenylalaninol) at the C-terminus. Interest in this antibiotic molecule (1) is generated by its ability to change the permeability of biological membranes by forming voltage-gated conductive channels (2). From studies on the concentration dependence of the conductances, it is known that 2–11 alamethicin molecules are involved in the transport of small metal cations through the membrane barrier (3,4). It is generally believed that the conducting state consists of amphipathic helical molecules that are associated in a transmembrane array forming the lining of an aqueous pore through which ions permeate. It is also assumed that the observation of multiple conductance states is related to changes in the size of the aggregate. The process of opening and closing the channels has been suggested to be based on the electric macro-dipole-dipole interactions between the individual helical peptide molecules in the closed channel and the effect of the membrane potential on the reorientation of the peptide dipoles to a parallel bundle of helices in the open channel. In the absence of charged peptide side chains, the helix dipole is the only source of electrostatic interaction with the membrane potential (4). The dipole moment of 75 Debye corresponds to a net charge of $+1/2$ charge at the N$-$ and a $-1/2$ charge at the C-terminus of the helix.

Three main models have been proposed to explain the molecular mechanism of the voltage gating. The peptide undergoes a voltage dependent reorientation either from a surface to a transmembrane orientation (3,5,6) or from an antiparallel to a parallel type of association (7). The peptide might also associate with the N-terminal helical domain inserted into the membrane as a barrel stave array, thereby leaving the nonhelical C-terminus outside the membrane, whereas the voltage-dependent step is thought to force the peptide bundle further into the membrane by extension of the helical conformation to the whole peptide chain (8–10).

In the absence of a membrane voltage, alamethicin is also capable to induce a liposomal leakage of carboxy fluorescein loaded vesicles (11). It was shown that water-membrane partition and aggregation phenomena are major determinants of the membrane activity of antimicrobial peptides. Even the transport of bulkier organic ions, like N^{α}-benzoyl-L-arginine-*para*-nitroanilide, was found to be induced by the membrane perturbing activity of alamethicin (12). In contrast to the transport of metal ions through multimeric peptide channels, the transport of N^{α}-benzoyl-L-arginine-*para*-nitroanilide is facilitated by monomeric alamethicin molecules.

Submitted September 22, 2008, and accepted for publication January 15, 2009.

*Correspondence: J.Raap@chem.leidenuniv.nl

Abbreviations used: Aib, α-aminoisobutyric acid; Alm-*n*, [Glu(OMe)^{7,18,19}]-TOAC spin-labeled alamethicin F50/5 at the *n*th position of the peptide sequence; cw, continuous wave; diPhPC, diphytanoylphosphocholine; DOPC, 1,2-dioleoyl-*sn*-glycero-3-phosphocholine; ePC, egg L-α-phosphatidylcholine; ESR, electron spin resonance; ESEEM, electron spin echo envelope modulation; Glu(OMe), γ-methyl ester of glutamic acid; LMV, large multilamellar vesicle; PELDOR, pulsed electron-electron double resonance; Phl, phenylalaninol; P/L, peptide to lipid; POPC, 1-palmitoyl-2-oleoyl-*sn*-glycero-3-phosphocholine; TOAC, 2,2,6,6-tetramethylpiperidine-1-oxyl-4-amino-4-carboxylic acyl; VMD, visual molecular dynamics.

Editor: David D. Thomas.

0006-3495/09/04/3197/13 $2.00

doi: 10.1016/j.bpj.2009.01.026

To understand the mechanism of ion channel and membrane leakage activities it is thus of interest not only to study the process of self-aggregation of alamethicin molecules in phospholipid bilayers, but also to determine the relative orientation of the peptide helices in the aggregate. In addition, the nature of self-association of helical peptides may provide information on the factors governing helix-helix association in membrane proteins. However, despite extensive research, our current understanding of the process of channel formation at the molecular level remains far from complete.

Solid-state NMR shed light on the 3D-structure of individual peptide molecules in the membrane-bound state (13–16). X-ray and neutron diffraction techniques have given information about the structure factor of the pore fluid, the influence of peptide on the phase and thickness of the membrane (17–24). Continuous wave ESR, together with paramagnetic spin-labeling techniques, has been used to study the molecular characteristics of alamethicin in lipid membranes (25–28). Above the lipid melting temperature, the transmembrane oriented alamethicin molecules were found not to be aggregated (26). However, below the transition temperature, the molecules appear to self-assemble. It was suggested that at room temperature ionic conductances arise from transient or voltage-induced molecular associations.

PELDOR is a reliable technique to measure interspin distances in the range of 1.5–8.0 nm. This technique allows one to obtain information about the length and the length-related secondary structure of a peptide from the magnetic dipole-dipole interaction between the nitroxide electrons of a double labeled peptide (29,30). A recent application of PELDOR to membrane-bound aggregated alamethicin molecules, each of them spin-labeled at both positions 1 and 16, allowed us to extract an intramolecular distance of 2.1 nm, which agrees with the distance in an approximately regular α-helical conformation, at least for the segment 1–16 (31).

However, if a monolabeled peptide is used, this technique provides information about the number of molecules as well as the intermolecular distances between the labels of the aggregate in hydrophobic solvents, which are assumed to mimic the interior of the lipid bilayer (32,33). The success of the latter approach was also shown in a preliminary PELDOR study of TOAC-labeled Alm in ePC membranes at 77 K (34). The number of molecules in the aggregate was determined and the intermolecular distance distribution function between the nitroxide radicals of the aggregated molecules was obtained.

The goal of this study is to elucidate the supramolecular structure of the alamethicin aggregate, in particular the relative orientations of the self-associated helical molecules and their orientation relative to the membrane surface, in membranes of LMV in the absence of an applied transmembrane voltage. This goal is achieved by site-specific spin-labeling of [Glu(OMe)^{7,18,19}] alamethicin F50/5: Ac-Aib–Pro-Aib-Ala-Aib-Ala-Glu(OMe)-Aib-Val-Aib-Gly-Leu-Aib-Pro-Val-Aib-Aib-Glu(OMe)-Glu(OMe)-Phl. Because both Aib and TOAC are strongly helicogenic, C$^{\alpha}$-tetrasubstituted α-amino acid residues (35–37), substitution of Aib at well-defined positions by TOAC is expected not to alter the 3D-structural properties of this molecule:

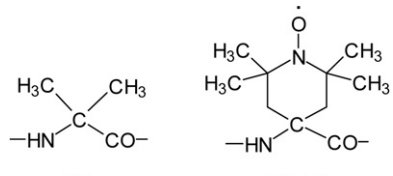

Aib TOAC

Indeed, substituting the three Gln residues in alamethicin F50/5 by Glu(OMe) was shown to have only minor effects on the conformation of the peptide chain (38,39) and ion channel formation as well (40).

Information on the distance distribution between spin-labels in membrane-bound aggregates was extracted from PELDOR data based on the magnetic dipole-dipole interactions between nitroxide spin-labels, which were determined at 77 K. Because CD and ESR studies showed that the aggregates are stabilized by lowering the temperature to near the transition temperature of the lipid (26,41), we assume that quickly freezing the samples (below the transition temperature of ePC, at ~270 K) does not affect the structure of alamethicin aggregates at 77 K.

We used the simplest version of the PELDOR technique (42,43), i.e., a usual two-pulse approach of the electron spin echo at frequency ν_A with addition of a pumping pulse at frequency ν_B. Two pulses at frequency ν_A form the spin echo signal. The pumping pulse is applied at time T after the first pulse. The pumping pulse at frequency ν_B rotates the spins belonging to another region of the ESR spectrum. This pulse changes the dipole-dipole interaction of some spins and, as a result, the amplitude of the spin echo signal, $V(T)$, starts to depend on both the magnitude of the dipole-dipole interaction between the spins and the strength and position (T) of the pumping pulse. This method makes it possible to separate the dipole-dipole interactions between spins from other interactions that substantially hamper this separation in the case of cw ESR and a conventional electron spin echo technique (43). Recently developed methods of PELDOR data analysis allow one to obtain a distance distribution function $F(r)$, which can provide detailed information on the distance between these spin-labels and about the aggregate number as well (44–50).

ESEEM spectroscopy (51) was used for the first time to probe the topology of the lipopeptide trichogin GA IV in the membrane (52). This result was achieved by comparing the ESEEM spectra with those known for lipids with spin-labels at different positions of the hydrocarbon chain (53–55). Because the amplitude of the ESEEM modulation of the spin-labels of the lipid appears to be strongly dependent on the presence of water molecules penetrating into the membrane, this technique was shown also to be useful to

estimate the membrane immersion depths of the spin-labels at different positions along the peptide chain.

In this study, the PELDOR study provides, to our knowledge, the first piece of experimental evidence for an approximately parallel alignment of ~4 aggregated alamethicin molecules in frozen ePC membranes. We report on the water accessibility of the same set of alamethicin analogs in ePC membranes. The geometrical results will be discussed according to a plausible penknife model.

MATERIALS AND METHODS

Materials

The solution synthesis and characterization of the TOAC spin-labeled [Glu(OMe)^{7,18,19}] alamethicins studied in this study are described elsewhere (56). The lipid extracted from egg-yolk (a mixture of phosphocholine lipids composed of C16:0/18:1 lipids as the major components) was purchased from Sigma (St. Louis, MO). Samples of LMV were prepared as described in Szoka and Papahadjopoulos (57). The complete sequences of the three peptides are:

Alm1: Ac-TOAC–Pro-Aib-Ala-Aib-Ala-Glu(OMe)-Aib-Val-Aib-Gly-Leu-Aib-Pro-Val-Aib-Aib-Glu(OMe)-Glu(OMe)-Phl;
Alm8: Ac-Aib–Pro-Aib-Ala-Aib-Ala-Glu(OMe)-TOAC-Val-Aib-Gly-Leu-Aib-Pro-Val-Aib-Aib-Glu(OMe)-Glu(OMe)-Phl; and
Alm16: Ac-Aib-Pro-Aib-Ala-Aib-Ala-Glu(OMe)-Aib-Val-Aib-Gly-Leu-Aib-Pro-Val-TOAC-Aib-Glu(OMe)-Glu(OMe)-Phl.

Sample preparation

Lipid and peptide mixtures at chosen P/L molar ratios were dissolved in chloroform. The solvent was removed by flush-drying with argon gas followed by high vacuum pumping at room temperature for 30 min. Note that at this stage alamethicin does not aggregate (32). After addition of the buffer [20 mM Tris·HCl buffer containing 140 mM NaCl and 1 mM EDTA (pH 7.0)] to the lipid film, the dispersion was equilibrated under argon at 4°C during 12 h for complete lipid hydration. A milky suspension of LMVs formed by a three-stage procedure of freezing, thawing and vortexing the hydrated lipid. To find the dependence of the $V(T)$ decay on the concentration of the spin-labeled sample, each of them was studied at different P/L ratios (1:70–1:200). The samples in ampules of 5 mm diameter containing ~80 μl of suspension were quickly frozen in liquid nitrogen and then used in the ESR and PELDOR measurements. Salnikov et al. (52) showed that the results of similar experiments do not depend on the speed of freezing. Three sets of experiments, which were carried out at different peptide concentrations, showed reproducible results.

ESR, PELDOR, and ESEEM spectroscopies

Continuous wave ESR spectra were recorded on an ESP-380 Bruker spectrometer. PELDOR studies were carried out using the PELDOR spectrometer that is described elsewhere (42,43). The durations of the first and the second pulses forming the spin echo signal were 40 and 70 ns, respectively. The duration of the pumping pulse was 30 ns. The position of the pumping pulse corresponded to the maximum amplitude in the ESR spectrum. The frequency difference ν_A-ν_B was 65 MHz. The intensity of the echo signal as a function of the T time interval between the first pulse and the pumping pulse [the PELDOR signal decay $V(T)$] was recorded. These decays were normalized to the magnitude of the echo signal in the absence of a pumping pulse. The other conditions for the measurement followed the protocols described in Milov et al. (34). ESEEM experiments were carried out at 77 K using an ELEXSYS E 580 spectrometer, which was equipped with a homemade low-Q resonator and a quartz Dewar filled with liquid nitrogen. This technique was carried out using a conventional three-pulse stimulated electron spin echo. The duration of the microwave pulses was 16 ns. The time delay between the second and the third pulses was incremented from 60 ns by 550 steps of 16 ns each, while maintaining the separation between the first and second pulses constant at 200 ns. Unwanted echoes were eliminated using the Bruker (Karlsruhe, Germany) Pulse Spel software, applying a four-step phase cycling program $+(0,0,0)$, $-(0,\pi,0)$, $-(\pi,0,0)$, and $+(\pi,\pi,0)$ (50). The D_2O modulation effects for peptide membrane systems were analyzed as described in Marsh (53) and Bartucci et al. (54,58). The spectrometer magnetic field was set to the maximum amplitude of the TOAC ESR spectrum.

Molecular modeling

A molecular model of the spin-labeled [Glu(OMe)^{7,18,19}, TOAC^{1,8,16}]-alamethicin F50/5 was derived from the x-ray diffraction structure of [Glu(OMe)^{7,18,19}, TOAC^{16}]-alamethicin F50/5 (39) using the HyperChem software (Hypercube, Gainesville, FL). For the computational details of the construction of the Alm F50/5 molecular model and the force field parametrization, we refer to our recent work on alamethicin (33). Four peptides (i.e., the aggregate) were aligned parallel according to a square arrangement and with the polar groups located at the inside of the peptide aggregate using the XMakemol software tool (version 5.16, copyright M. P. Hodges, 2007, free download at http://www.nongnu.org/xmakemol/WelcomePage.html). The peptide aggregate was placed in a periodic cubic box with edges of 10 nm, large enough to ensure that the periodic images do not interact. A series of constraint energy minimizations were carried out using the OPLSAA force field (59,60), where the force field parameters for TOAC molecular moiety were obtained from Parsegian et al. (61). The long-range interactions were computed up to 2.0 nm using a simple cut-off scheme. The constraints were simple square-well potentials with a variable well range. We constrained the intermolecular distances between the exocyclic oxygen atoms of the 1, 8, and 16 TOAC alamethicin analogs. For each peptide, we had $3 \times 2 \times 1 = 6$ constraints, and hence a total of 18 constraints for the aggregate. We started with a minimum well value (r_{min}) of 1.5 nm and a maximum (r_{max}) of 3.5 nm. We kept r_{max} fixed and increased r_{min} in steps of 0.1 nm, i.e., 1.5, 1.6, 1,7, etc. After every update of r_{min}, we minimized the geometry up to a target gradient of 0.01 kcal/mol Å. In this way we found a minimum of the potential energy at $r_{min} = 1.8$ nm. The resulting structure was used for further analysis. Note that the potential energy increase due to the constraints was never larger than a few kcal/mol. The dimensions of the supramolecular model structure were compared to those of the gel phase ePC membrane (3.5 nm for the hydrophobic core and 4.7 nm for the total thickness). These latter values were obtained from the x-ray diffraction data of ePC fluid membranes (62), which were corrected to the gel phase dimensions by a conversion factor of 1.34 and 1.24, respectively (63).

RESULTS

Continuous wave ESR spectra

Fig. 1 shows the cw ESR spectra of the spin-labeled analogs of alamethicin bound to membranes of the ePC vesicles, which were frozen at 77 K. For comparison, the ESR spectrum of Alm1 (2×10^{-3} M) in frozen glassy methanol/ethanol solution is also shown. In the latter case the dipole-dipole interaction of the spin-labels is weak and no broadening is shown in the ESR lines, whereas the lines of the ESR spectra 2-4 of Alm in ePC vesicles are remarkably broadened. This effect can be attributed to aggregation of Alm in the vesicles. Furthermore, it should be noted that the shape of the spectra is indicative of the occurrence of

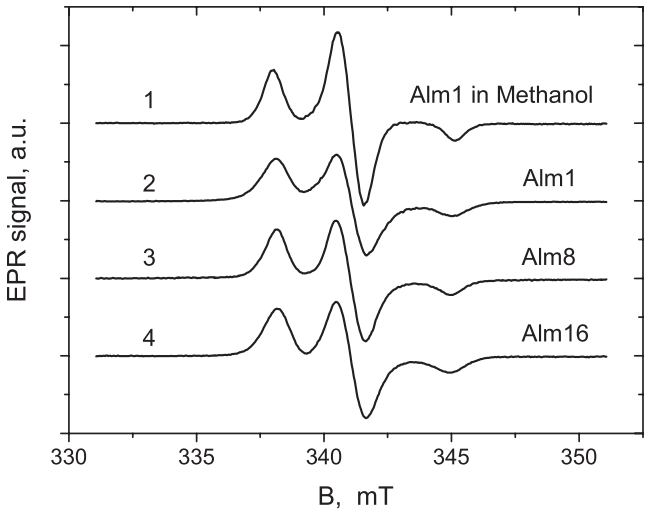

FIGURE 1 Continuous wave ESR spectra of spin-labeled alamethicin analogs at 77 K. Curve 1: Alm1 (2×10^{-3} M) in methanol (containing 5% ethanol). Curves 2–4: Alm1, Alm8, and Alm16 in ePC vesicles at a P/L molar ratio of 1:150.

disordered nitroxyl radicals in the solid phase. Both the shape and widths of the cw ESR lines clearly indicate the absence of intermolecular distances for the spin-labeled specimens <1.5–1.6 nm (64). The spectra appear only slightly dependent of the peptide concentration (not shown).

PELDOR of the spin-labeled alamethicin analogs in ePC vesicles

Fig. 2 *A* shows the experimental decays of the PELDOR signal, $V(T)$, for the alamethicin analogs in frozen LMVs. Curves 1 and 2 refer to the Alm1 analog with a P/L molar ratio equal to 1:70 and 1:160, respectively. Curves 3 and 4 were recorded using the Alm8 and Alm16 analogs, which were bound to the membranes at the P/L molar ratio of 1:70. Two characteristic regions can be distinguished in the $V(T)$ decays: i.e., in the region of low T ($T < 100$ ns), a rapid decay of $V(T)$ is observed, whereas at $T > 100$ ns a relatively slow decrease of the signal is found, which seems to be peptide concentration dependent. This dependence is shown for Alm1 in curves 1 and 2 of Fig. 2 *A*. Similar dependences in the same interval were recorded for Alm16 and Alm8 (not shown). Another example of such a behavior of the PELDOR signal decay at different concentration of Alm16 was reported previously (35).

The rapid initial decay of $V(T)$ is indicative of the presence of aggregates of monolabeled molecules in the sample. The depth of the decay depends on the spin-label location in the peptide molecule. The fastest decrease of the signal is observed for Alm16, whereas for the Alm8 and Alm1 analogs slow initial decays are recorded. Thus, a tentative conclusion can be drawn that the fraction of spin-labels with relatively short distances decreases in the order Alm16 > Alm8 ≈ Alm1. It is worth noting that aggregation takes place during binding of this peptide to the membrane and not during the earlier steps of the vesicle preparation (31). The slow decay at $T > 100$ ns may originate either from dipole interactions of the labels inside the aggregate, or from interactions between the labels of different aggregates and nonaggregated molecules (if any).

To separate the contributions of intra- and interaggregate interactions into $V(T)$, we assume that these contributions are independent. The value of V_{INTRA} depends on the structure of the aggregate and is independent of the peptide concentration, whereas V_{INTER} depends on the P/L ratio. Thus, the total value of $V(T)$ represents the product $V_{INTRA}V_{INTER}$ (43). The dependence of V_{INTRA} (T) was derived as described in Milov et al. (45), by elimination of the concentration dependent contribution to the experimental signal decay. To this end, the experimental decay, obtained for two different peptide concentrations, can be used to derive the intra-aggregated part V_{INTRA} (T). To derive V_{INTRA} (T), we used the relation $\ln(V_{INTRA}) = (C_2 \ln V_1 - C_1 \ln V_2)/(C_2 - C_1)$, where V_1 and V_2 are the $V(T)$ decays at peptide concentrations C_1 and C_2, respectively. The mean value of V_{INTRA} (T) was obtained by using three pairs of C_1 and C_2 values for the P/L ratios in the range of 1/70–1/200. All combined V_{INTRA} data are shown by dots in Fig. 2 *B*. The overlaid solid curves were calculated from the distance distribution functions over the distances between the labels in the aggregates shown in Fig. 3 (see below).

Distance distribution functions and number of labels per aggregate

The distance distribution for the spin pairs is denoted as $F(r) = dn(r)/dr$, where $dn(r)$ is the fraction of peptide molecules with distances between the spin-labels ranging from

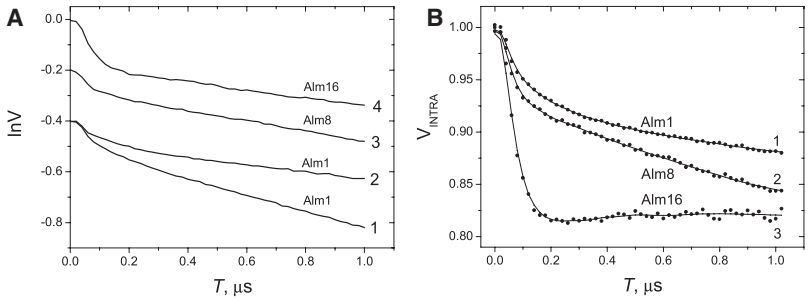

FIGURE 2 (*A*) PELDOR signal decays for spin-labeled alamethicin analogs bound to the membranes of ePC vesicles at 77 K. The P/L molar ratio is 1:70 for curves 1, 3, and 4, and 1:160 for curve 2. Curves 1 and 2 are shifted downward by 0.4 and curve 3 is shifted downward by 0.2. (*B*) V_{INTRA} signal decays for frozen solutions of alamethicin analogs in ePC vesicles.

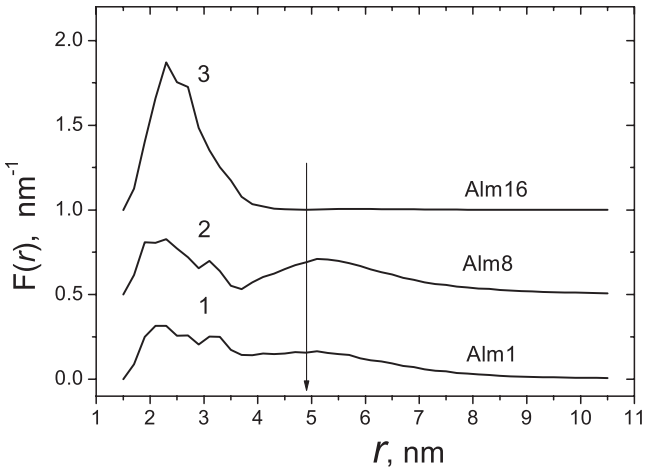

FIGURE 3 Distance distribution functions $F(r)$ between spin-labels for alamethicin analogs in membranes of frozen ePC vesicles. Curves 2 and 3 are shifted upward by 0.5 and 1.0, respectively. The distance distributions are obtained from the experimental V_{INTRA} decays by the Tikhonov regularization method. The shape of $F(r)$ at larger distances than that indicated by the arrow is not authentic and can be used for the estimation of the area in this r-region.

r *to* $r + dr$. The $F(r)$ form was obtained by comparing the experimental and calculated V_{INTRA} decays. According to Milov et al. (34), the expression for V_{INTRA} in the case of N spin-labels per aggregate, can be given as

$$V_{\mathrm{CALC}} = 1 - (N-1)p_b \int_{r_1}^{r_2} F(r)(1 - f(r,T))dr, \quad (1)$$

where T is the delay between the first pulse and the pumping pulse, r is the distance between the labels, the function $f(r,T)$ describes the signal oscillations due to the dipole-dipole interaction between two labels, and the p_b value refers to the probability of the spin flip induced by the pumping pulse. From Eq. 1, at large T values the function $f(r,T) \rightarrow 0$ and the following relation between N and $V_{\mathrm{INTRA}}(T \rightarrow \infty)$ holds: $(N-1)p_b = 1 - V_{\mathrm{INTRA}}(T \rightarrow \infty)$. Under these conditions the value $(1 - N)$ can be determined experimentally. The integration limits r_1 and r_2 define a physically reasonable range of distances between the spin-labels in the aggregates. Equation 1 is valid if p_b is independent of r, which holds for $r > 1.6$ nm. For such distances, the broad line of the ESR spectrum is of minor importance.

As follows from Fig. 3, $V_{\mathrm{INTRA}}(T)$ displays a significant decay of the PELDOR signal at T values <100 ns, i.e., at times comparable with the duration of the mw pulses. This result indicates that for Eq. 1 one should take the effects of both the duration of the mw pulses and the location of the spin-label frequencies in the ESR spectrum into account. Thus, in our subsequent analysis, the values of $V(0)$, p_b, and $f(r,T)$ were calculated from the relations derived in Maryasov and Tsvetkov (65). In this case, the duration of the pulses was taken into account and the averaging was carried out over the orientations of the spin-labels and their frequencies in the ESR spectrum.

By substituting the integral in Eq. 1 by the sum and setting a theoretical expression of V_{CALC} equal to the experimental dependence of V_{INTRA}, we derive the following linear equations:

$$\sum_{k=1}^{m} X_k K_{jk} = U(T_j), \quad (2)$$

$$X_k = p_b(N-1)F(r_k)dr_k, \text{ and} \quad (3)$$

$$K_{jk} = \int_{r_k}^{r_k + dr_k} \left(1 - f\left(r, T_j\right)\right)dr/dr_k, \quad (4)$$

where X_k are unknown values, $U(T_j)$ are determined experimentally, and $U(T_j) = 1 - V_{\mathrm{INTRA}}(T_j)$. The number of equations in Eq. 2 is equal to the number of the experimental points T_j.

The method developed by Tikhonov, which is known as the ''Tikhonov regularization'' method for solving ill-posed problems (49,66), can be used effectively to obtain a distribution function from Eqs. 2–4. The method allows one to derive a solution for the set of linear Eq. 2 for which $U(T_j)$ is determined with some errors with respect to its exact values. In terms of the Tikhonov method, the solution was obtained by varying the X_k values included in Eq. 2 with $X_k \geq 0$ to numerically minimize a functional M of the form

$$M = R^2 + \lambda\Omega^2, \quad (5)$$

where $\lambda \geq 0$ and the values R and Ω obey the relations

$$R^2 = \sum_{z=1}^{n}\left(\sum_{k} X_k K_{jk} - U(T_j)\right)^2; \Omega^2 = \sum_{k=1}^{m} X_k^2. \quad (6)$$

Here, n is the number of experimental points (at the T-scale), m is the number of points over the distance scale r, and λ is the Tikhonov regularization parameter (49,66). To solve the problem of finding $F(r)$, the range of distances from 1.4 to 10.4 nm was split into regular intervals, with steps of 0.2 nm. The lower limit of the range ($r_1 = 1.4$ nm) corresponds to distances that can be determined by PELDOR with regard to the mw pulse duration (34). The upper limit of the r_2 value was chosen using the relation $\frac{\gamma^2\hbar T_{\max}}{r_2} \cong 0.3$, where $T_{\max} = 1\ \mu$s is the largest experimental value for the delay T. Note that the region of the reliable behavior of $F(r)$ is limited by the distances for which the dipole-dipole interaction is strong enough, i.e., $\frac{\gamma^2\hbar T_{\max}}{r^3} \cong \pi$. This relationship corresponds to a distance of ~5 nm (shown by the arrow in Fig. 3). In the distance range of 5–10.4 nm we derive a formal solution to $F(r)$, which corresponds to a tolerant solution of the incorrectly formulated problem. The optimum value of λ in Eq. 5 is 0.3.

Fig. 3 shows the $F(r)$ functions for all three spin-labeled analogs of alamethicin in the frozen LMV suspension, obtained by the described method. The PELDOR signal decays, calculated from these distribution functions, are shown in Fig. 2 *b* by solid lines. The curves 1, 2, and 3 in Fig. 2 *B* show that the distribution functions are in a good agreement with the experimental data (shown by *dots*).

Characteristic properties of the distribution functions

The distance distributions, shown for Alm1 and Alm8 in Fig. 3, exhibit two groups of lines. The first one is situated in the region of short distances ($r < 3.5$ nm) with a maximum at 2.3 nm and the second one is in the region of longer distances ($r > 3.5$ nm) with a maximum of ~5.2 nm. Only the first group of lines, with a maximum at 2.3 nm, is observed for Alm16. Therefore, the distance distributions observed are a superposition of two groups of lines with different relative intensities depending on the spin-label position in the alamethicin analog. The maxima of these groups of lines, together with the ratio between the areas of those lines, are the main parameters that determine the possible structures of the aggregates of the alamethicin analogs in ePC vesicles. It is necessary to keep in mind that, due to the special features of the Tichonov solution, the shape of $F(r)$ at long distances ($r > 5$ nm, indicated by the arrow in Fig. 3) is not authentic and can be used only for estimating the area in this region of distances.

It should be noted that for Alm8 the two groups of lines do not overlap. After integration, a ratio of ~2:3 was obtained for the areas of the first and the second group of lines. The distance distribution function shown for Alm1 (Fig. 3, *curve 1*), however, shows some overlap of these groups. Nevertheless, estimation of the areas can be obtained if we take the similarity of the different line shapes for Alm1 and Alm8 into account. The estimated ratio of the areas for Alm1 also appears to be ~2:3.

Estimation of the number of spin-labels in the aggregates

To estimate the number of spin-labels we assumed that all aggregates contain the same number of Alm molecules. This value was derived by the following two methods:

1. By solving Eq. 2 to obtain the value of $(N - 1)\,p_b$, from which the aggregate number N can be estimated. Taking into account that $\sum_k F(r_k)dr_k = 1$, from Eq. 3 we derive $N = \frac{1}{p_b}\sum_k X_k$. The p_b value was calculated by using the relations given in Maryasov and Tsvetkov (65). This method for the estimation of the aggregate number was already described (34). As a result, N was calculated to be 3.5, 4.4, and 4.3 for Alm1, Alm8, and Alm16, respectively. These values indicate that the aggregate number is close to four. Note that the value of N estimated by this method includes experimental errors and a systematic error (that is difficult to take into account) originated by the choice of the optimal parameter in the Tikhonov regularization.
2. By calculating N directly from the experimental asymptotic value of V_{INTRA} at large T for Alm16. According to Eq. 1, at large T the value of V_{INTRA} tends to $V_p = 1 - (N - 1)\,p_b$. Fig. 2 *B* shows that this estimation can only be carried out for Alm16, for which V_{INTRA} tends to the limiting value $V_P = 0.82 \pm 0.02$. From the resulting value $p_b = 0.054 \pm 0.002$, we derive $N = (1 - V_P)/p_b = 4.3 \pm 0.6$. Thus, the value of N obtained by both methods is close to four. One possible reason for underestimating the number of subunits in the aggregate, namely peptide underlabeling, is not operative here because none of the steps used for the synthesis in solution of these peptides involves the acidic chemical conditions undermining the nitroxide label survival.

ESEEM experiments of spin-labeled alamethicin analogs in ePC: the interaction of spin-labels with the nuclei of deuterated water

Curve 1 of Fig. 4 *A*, shows the three-pulse spin echo decay for a frozen sample of Alm1 in ePC vesicles that were hydrated in D_2O buffer. The data are presented with regard to the delay t between the second and the third pulses forming the echo signal. In this case, the delay between the first and the second pulses, τ, remained constant. An increase in t results in the decay of the stimulated echo signal with a strong modulation. The oscillation frequency of this modulation is close to the resonance frequency of the deuterons in the magnetic field of the spectrometer (~2 MHz). Similar dependences, but with smaller modulation amplitudes,

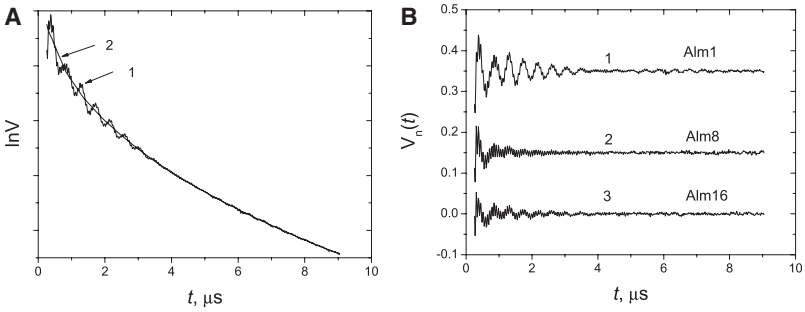

FIGURE 4 (*A*) ESEEM decays for Alm1 bound to membranes of D_2O-hydrated ePC vesicles. The stimulated echo signal (V) dependence on the delay between the first and the third pulses, t, is shown in curve 1. Curve 2 is smoothed by a six-order polynomial. (*B*) The normalized spin echo dependence on the delay time t for spin-labeled alamethicin analogs in ePC vesicles hydrated in D_2O buffer. The P/L molar ratio is 1:70. The spin echo signal V_n is normalized.

were also obtained for Alm8 and Alm16 (not shown). In previous data published in Marsh (53), Bartucci et al. (54), and Erilov et al. (55), the modulation induced by the deuterium nuclei was observed in stimulated ESE for spin-labels in phospholipid vesicles prepared in the D_2O buffer. In this case, the modulation amplitude was substantially dependent on the accessibility of the labels for the D_2O molecules.

The spin echo signal decay, depending on t, is determined by the processes of relaxation that are independent of the modulation phenomena, and thus can be eliminated. According to Bartucci et al. (54,58) and Erilov et al. (55), the modulation effects can be distinguished by using a normalized echo signal $V_n(t)$:

$$V_n = V(t)/\langle V(t)\rangle - 1,$$

wherein $\langle V(t)\rangle$ is the smoothed dependence $V(t)$. Curve 2 in Fig. 4 *A* is $\ln\langle V(t)\rangle$, obtained by the smoothing of curve 1 by a six-order polynomial. This procedure removes the monotonic component of the decay from the time trace of the echo decay function.

Fig. 4 *B* shows the normalized echo signals for different spin-labeled alamethicin analogs bound to ePC membranes. The largest amplitude of the deuterium modulation is observed for Alm1. For the Alm8 and Alm16 analogs, the deuterium modulation is smaller and close to the amplitude with a high-frequency ($\cong$14.6 MHz) modulation, induced by protons. The data allow a qualitative conclusion that the aggregates of the alamethicin analogs are oriented in the ePC bilayer so that the spin-labels at the first position are closer to the water-lipid interface than those at positions 8 and 16.

DISCUSSION

Aggregate number of molecules estimated from PELDOR spectroscopy

To construct the structure of the membrane bound peptide aggregate, it was necessary to know the number of peptide building blocks. Thanks to our previous PELDOR investigation of aggregates of the lipophilic peptide trichogin GA IV (32) and the study of structurally semirigid and well-defined bi-, tri-, and tetraradicals (50), the method to analyze the aggregate number is well established. In the latter study it was shown that dimers, trimers, and tetramers can be distinguished readily. In this study, the aggregate numbers were estimated by using two different methods to analyze the V_{INTRA} decays (shown in Fig. 2 *B*). From the Alm1, Alm8, and Alm16 samples the number of N peptide monomers was estimated to $N = 4.1 \pm 0.4$, respectively, whereas $N = 4.3 \pm 0.6$ was obtained from Alm16 by using an independent method.

At this point the question should be addressed whether this variability is due to an error of analysis or to the presence of a heterogeneous assembly of aggregates built from a mixture of three, four, and five molecules. In patch clamp studies the variation of multiconductances, dependent on the lipid chain length and P/L ratio was indeed interpreted in terms of a variable N (3,4). Unfortunately, a quantitative comparison of the aggregate numbers is complicated by the fact that in the latter studies the kinetics of the voltage-gated opening and closing of alamethicin channels were investigated, whereas in our work the thermodynamically stable structure of the closed state of the aggregate is studied. Nevertheless, the interpretation in terms of an average value of N due to the presence of a mixture of trimer/tetramer/pentamer aggregates seems very unlikely in view of a molecular dynamics study of alamethicin barrels of different sizes (67). The latter study showed that their stabilities follow the order: tetramer $<$ pentamer $<$ hexamer. By following this trend it might thus be anticipated that trimers are less stable than tetramers and consequently the concentration of trimer would be much less than the amount of pentamer. Thus, the assumption of the presence of the same amounts of trimers and pentamers (at P/L values ranging from 1:70 to 1:160), equally contributing to the mean aggregate number ($\langle N\rangle = 4$), does not seem reasonable.

Structural information from PELDOR

We used the PELDOR technique to obtain geometric information about the self-assembled supramolecular structure of the pore forming alamethicin analogs. An important observation of the distance distribution curves shown in Fig. 3 is that, independent of the label position, similar distance distributions are found ~2.3 nm. This finding agrees with a simple model of a parallel alignment of a face-to-face type of helix-helix association with the polar groups oriented to the inside and with the spin-labels located at the outside, but disagrees with an antiparallel orientation. In the latter case the theoretical distance between the TOAC-16 labels would be 3.4 nm, which is at the extreme side of the experimental distance distribution curve 3 (Fig. 3).

To further study the helix-helix interactions in more detail, a molecular modeling study was carried out. In this investigation a set of distance restraints was used that was taken from the intermolecular PELDOR distances between the TOAC labels. For convenience, but in contrast to the actual experiments, each peptide molecule was labeled threefold, at the 1, 8, and 16 positions (see the ''Molecular modeling'' paragraph in the Materials and Methods section for details). In Fig. 5 the computed gas-phase energy minimized structure shows a peptide complex that is built from four parallel, but slightly tilted α-helices. A more detailed examination of the aggregate structure shows that all peptide helices are more or less perturbed due to the missing hydrogen bonds at the helix breaking region Gly^{11}-Pro^{14} (the bending angles of the *blue*, *red*, *cyan*, and *yellow* colored chains are 151°, 150°, 130°, and 125°). It is worth noting that bending of the peptide helix has also been found in a ^{1}H-NMR study of micelle-associated alamethicin (68).

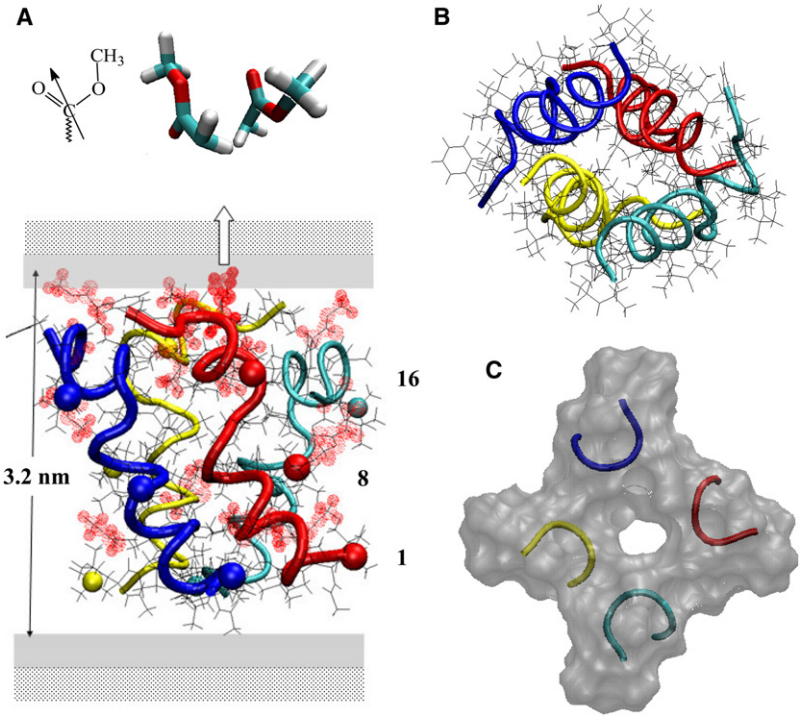

FIGURE 5 Energy minimized model of the supramolecular alamethicin tetramer, which is based on the short 2.3 nm PELDOR distance between the exocyclic oxygen atoms of the TOAC-1, TOAC-8, and TOAC-16 spin-labels. The spatial positions of the oxygen radicals are indicated by balls, with the TOAC-1 labels shown at the bottom of the figure. For clarity, but in contrast to our experiments, each peptide is threefold labeled. (*A*) A side view of the tube model shows the spatial arrangement of four parallel aligned α-helical peptide chains, which make angles of -15° (*blue* and *red chains*), $+13^\circ$ (*cyan chain*), and -8° (*yellow chain*), with respect to the membrane normal. The helices are bent at the Leu^{12}-Aib^{13} sequence due to the missing hydrogen bonds between the carbonyl oxygens of the Gly^{11} and the tertiary nitrogen atoms of the Pro^{14} residues. The maximum diameter of the peptide complex (3.2 nm) appears roughly matching the hydrophobic thickness of the membrane double layer (3.5 nm). For convenience, the zwitterionic and polar regions of the membrane are also depicted. The locations of the flexible polar side chains of the γ-ester groups of the Glu(OMe)^{7,18,19} residues are shown by dotted balls. A more detailed arrangement, particularly for the (Glu(OMe)^{18} residues of the red and cyan colored peptide chains, is shown in the inset of *A*. These mutually antiparallel oriented γ-ester groups are located at a distance of 0.36 nm. The electric dipole-dipole interactions between the ester groups are believed to stabilize the C-terminal ends of the peptide chains. This stable region of the peptide complex might be further supported by the relative narrow PELDOR distribution of distances found for TOAC-16. (*B* and *C*) Top down views of the peptide complex (the N-terminal ends are shown at the front side). (*B*) Tube model of the spatial arrangement of the helical chains. (*C*) A semitransparent surface model of a thin slice with a thickness of about half of a helix-turn and showing the entry of one or more channels within the tetramer.

To confirm whether the α-helical conformation of the associated peptide molecules of the supramolecular model shown in Fig. 5 is correct, the nonrestrained *intra*molecular distances between TOAC-1 and TOAC-16 of the model were compared with the corresponding experimental distance determined previously by PELDOR for ePC membrane bound aggregates of the double labeled F50/5 [Glu(OMe)^{7,18,19}, TOAC^{1,16}]-alamethicin analog (31). In the latter study the average of the *intra*molecular distance between these two labels was found 2.1 ± 0.1 nm (with a deviation of 0.5 nm for each of the peptide molecules of the ePC bound aggregate), independent of the P/L ratios, i.e., P/L 1:50 and P/L 200. The comparison indeed shows that the theoretical distance matches the experimental one (within experimental error), despite the perturbation induced by the Gly^{11}-Pro^{14} sequence. Thus, the conformation of the membrane bound peptides is likely to be α-helical.

Further inspection of the model shows that the *inter*molecular distances between the exocyclic oxygen atoms of the TOAC residues (1.8 nm) fall within the first peak of the PELDOR experiments, but not at the maximum of 2.3 nm. Clearly, our minimalist gas-phase model is flawed here (vide infra). Next, the model structure was oriented with respect to the membrane normal by adjusting the parallel aligned N-terminal helices to tilt angles of -15° (*blue* and *red colored chains*), $+13^\circ$ (*cyan*), and -8° (*yellow*), in a similar manner as was found in ESR and solid-state NMR studies of alamethicin (16,27,29). According to Fig. 5, the lengths of the blue, red, and yellow colored transmembrane helices (~3.2 nm) are likely matching the hydrophobic thickness of the ePC membrane (~3.5 nm), in view of the uncertainty of the applied conversion factors to calculate the thickness of the membrane (61,63) and the possibility of peptide induced membrane thinning effects (22). The C-terminus of the cyan colored chain, however, is immersed more deeply into the hydrophobic region of the membrane.

Finally, the positions of the polar Glu(OMe)^{7,18,19} residues with respect to the different hydrophobic, polar, and zwitterionic choline regions of the membrane might be of interest in view of their possible role in the closed (nonconducting) state of the alamethicin channel. In Fig. 5 these positions are indicated by dotted circles, schematically suggesting their uncertainties due to the flexibilities of the γ-ester side chains. Four out of a total of eight of the C-terminal residues are located in or nearby the polar lipid ester region of the membrane, whereas the remaining residues are buried more deeply. The inset at the top of Fig. 5 shows that the two carbonyl esters of the Glu(OMe)^{18} side chains of the red and cyan chains are mutually located at a distance of 0.36 nm. It should be noted that in our previous investigation of aggregates of Alm1, Alm8, and Alm16 in hydrophobic solvents (to mimic the hydrophobic interior of the membrane), the electric dipole-dipole interactions between the γ-ester groups were found to be the key determinant to

stabilize the peptide complex. Thus, it seems that the association of the C-termini of the peptide cluster in the ePC membrane is stabilized in a similar manner. One might also speculate about the role of the γ-ester groups of the Glu(OMe)[19] residues to anchor the aggregate to the polar region of the membrane by dipole-dipole interactions with the surrounding lipid ester groups.

In view of our interest in the functioning of the alamethicin-induced ion channels, Fig. 5 (*insets B* and *C*) is relevant to discuss. Further inspection of thin slices of the model along the *z* axis shows indeed the presence of one or more microchannels. In Fig. 5 *C* of the transparent surface model of a thin slice (at a thickness of about half of an α-helical turn) the entry of the N-terminus of the aggregate is shown. It should be recalled, however, that the intermolecular OR-OR ester distances (1.8 nm) in our model are slightly shorter than the r_{max} (2.3 nm) values observed by PELDOR. Thus, in the membrane-bound aggregate the distances between the helices might be extended by ~0.5 nm and, as a result, the actual size of the microchannels might be slightly larger than those in our model. It is worth noting here that water filled pores were also found in neutron and x-ray diffraction studies of alamethicin incorporated into fluid planar membranes, but at higher peptide concentrations as those used in our study (17,23,24).

Four Glu(OMe)[7] side chains are shown at the center of the hydrophobic core of the membrane. It should be emphasized, however, that the current model has not been simulated in a lipid environment and for this reason the accurate positions of the flexible polar ester side chains, in particular those at positions 7, are still uncertain.

At this point of the discussion, it is important to note that the experimental distance distributions exhibit multiple (2.3, 3.2, and 5.2 nm) distances for Alm1 and Alm8, whereas for Alm16 only a relative short distance (2.3 nm) was found. Due to the application of 2.3 nm distance restraints during our energy minimization, it is not surprising that the distances of ~3.2 and 5.2 nm observed by PELDOR for Alm1 and Alm8 are not reproduced during the molecular modeling. Because distances of the order of 3.2 and 5.2 nm are not observed experimentally for the TOAC-16 labels, the possibility of aggregates located at opposite leaflets of the membrane can be readily discarded. Other options, like for instance peptide induced nanorafts, local phase transitions of the membrane or extending the peptide aggregate structure from one bilayer to another in a multilayered vesicle (18–20), seem also not reasonable.

Further inspection of the distance distribution curve of Alm8 shows that the short and long distances are separated by a minimum at 3.7 nm. This finding indicates that the N-termini of the chains are not randomly unordered. To propose a structure that would be consistent with both short and long distances between the TOAC-8 and TOAC-1 labels, we examined two different structures according to a penknife model (Fig. 6). First, the option $\alpha = 180^\circ$ was considered. However, the energy minimized structure, obtained by using 5.2 nm distance restraints for two TOAC-1 labels of chains oppositely situated in the aggregate structures, turns out not to be realistic for a membrane bound aggregate. The distance of 5 nm is apparently too long to match also the total thickness of the membrane. Furthermore, in such a structure the eight polar Glu(OMe)[18,19] residues would be at the center of the peptide complex, a situation that seems to be very unlikely.

Next, we examined the option $\alpha = 90^\circ$, i.e., a T-shaped model, built started from standard α-helical molecules by using the VMD software and keeping the distances between all TOAC-16 labels constant (2.3 nm). The T-shaped structure might be formed by a transmembrane dimer in association with an in-plane associated dimer. The long-range distances of 4.8–6.4 nm between TOAC-1 and 4.0–4.4 nm between TOAC-8 labels are qualitatively in agreement with the PELDOR distances. Although this structure seems rather fragile, the joint between the transmembrane dimer and the surface associated dimer might be stabilized by the electric dipole-dipole interactions between the γ-ester groups of the Glu[18,19] residues as well as by stacking of the phenyl rings and hydrogen bonding of the alcohol groups of the C-terminal Phl residues[20]. However, in the absence of a reliable starting structure for a T-shaped-like structure, a molecular dynamics simulation would be extremely difficult. For this reason, we decided to carry out ESEEM experiments to get a better insight into the possibility of different (co-existing) quaternary structures.

Membrane-related topology of the aggregates of alamethicin analogs from ESEEM

The experiments were carried out by using Alm1, Alm8, and Alm16 in membranes of ePC vesicles, which were prepared in D_2O. Because the amplitude of the ESEEM modulation of the spin-labels seems to be strongly dependent on the water profile of the membrane, this technique was used to investigate the immersion depths of the different spin-labels of the aggregate with respect to the membrane surface. An analysis of the modulation amplitudes shown in Figs. 4, *A* and *B*, revealed that the water accessibility of the spin-labels situated in the ePC membrane follows the order Alm1 >> Alm8 ≈ Alm16, which is in agreement with experiments reported previously with mono-unsaturated (POPC) lipid membranes at 77K (18). The simplest interpretation of this observation is that the labels at the N-terminal positions are situated more closely to the lipid-water interface, whereas the labels at positions 8 and 16 are more buried. However, in the aggregate model shown in Fig. 5 the TOAC-1, TOAC-8, and TOAC-16 labels are separated from the membrane surface on the average by ~0.5 nm, 1.4 nm, and 0.9 nm, respectively. Thus, from this information one would expect the order of water accessibility to be TOAC-1 > TOAC-16 > > TOAC-8. However, if we take the water molecules

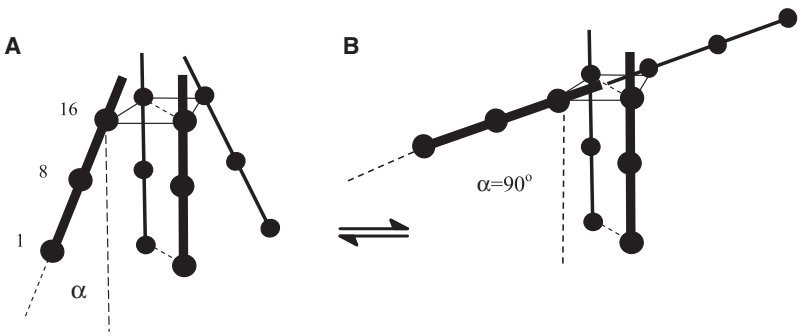

FIGURE 6 (*A*) Schematic representation of the model characterized by a penknife type of association, i.e., two parallel aligned transmembrane peptides, whereas two other peptide chains are making an angle α. Distances between the TOAC-16 labels, indicated by solid lines, are kept fixed at 2.3 nm. The positions of the spin-labels along the schematic peptide chains are shown by balls. (*B*) The T-shaped tetramer structure, defined by $\alpha = 90°$, qualitatively explains the occurrence of both the short and long experimental distances between the TOAC-1 and TOAC-8 labels of 2.3 + 3.2 nm and 5 nm, whereas for TOAC-16 a distance of ~2.3 nm only was found. Together with the water accessibility of the labels estimated by ESEEM spectroscopy, the combined data might be understood by considering the presence of two types of aggregated species, corresponding to $\alpha = 0°$ (transmembrane tetramer) and $\alpha = 90°$ (T-shaped complex).

accommodated at the center of the channel into account, the order might be TOAC-1 > TOAC-8 ≈ TOAC-16.

The same order of water accessibility, however, can be understood from the T-shaped model shown in Fig. 6, wherein the TOAC-8 labels are situated at the center as well as at the surface of the bilayer. Thus, the water accessibility as well as the PELDOR distances can be rationalized in terms of the T-shaped model. However, as we will see below, it is not reasonable to assume that the T-shaped tetramer would occur as the only membrane-bound species.

As is shown for the curve of Alm8 in Fig. 4, the areas for the narrow (1.6–3.2 nm) and broad (4.6–5.9 nm) PELDOR distance distributions are better resolved than those for Alm1 (ratio 2:3) (see the ''Characteristic properties of the distribution functions'' subsection of Results). This experimental ratio of the areas is then related to the statistical distribution of the numbers of small (N_S) and large (N_L) distances in the model. Because for the T-shaped model the long distances are too dominating ($N_S/N_L = 1:5$) compared to the approximated experimental ratio of 3:2, a complex model is considered, wherein short and long distances are more balanced. Let us assume a frozen equilibrium of a T-shaped tetramer together with a transmembrane tetramer, wherein the fraction of the parallel tetramer in the mixture is defined as x and that of the T- shaped tetramer as $(1 - x)$. The overall ratio between the numbers of the small and long distances in both models is then $(6x + 1(1 - x))/5(1 - x)$, which equals the experimental ratio of 2:3. From this simple relationship, x is found to be ~0.28. In conclusion, the model wherein transmembrane and T-shaped tetramers coexist in the membrane might satisfy the experimental distances between the labels, the statistics of the number of the experimental label distribution as well as the qualitative water accessibility of the labels.

Oriented circular dichroism studies of alamethicin in planar diPhPC membranes suggested that, dependent on peptide concentration, the transmembrane I-state as well as the surface-bound S-state might coexist in alamethicin (69). However, at room temperature the level of aggregation for the two different states is not clear yet. Thus in the case of a major population of monomers the PELDOR signal contributions due to these concentration dependent I and S species would be eliminated by the separation of the V_{INTER} and V_{INTRA} decay functions. At the present state of our research the exact nature of the complex of two differently membrane associated molecules, as shown in the tentatively proposed T-shaped model, remains an open question. Depth-dependent fluorescence quenching of spin-labeled lipid probes and polarized attenuated Fourier transform infrared experiments with unilamellar vesicles of ePC/cholesterol (1:1) demonstrated that the N-termini of the aggregated Alm molecules adopt different orientations with respect to the membrane normal (70). Thus, the latter observation might confirm a penknife type of spatial rearrangements of the self-assembled helical molecules, in a similar manner as was proposed for the rearrangement of the transmembrane helices of the pore-forming protein colicin (71–73). In contrast to our experiments carried out in ePC vesicular membranes, however, solid-state NMR experiments of [U-^{15}N]-alamethicin reconstituted in oriented planar POPC membranes showed mainly transmembrane oriented species at 248 K (18).

At this point the question arose whether the tetramer aggregates studied are relevant to understand the closed (nonconducting) state of the alamethicin channel. First, it is important to recall that the Glu(OMe)[7,18,19] alamethicin analogs are capable to form functional channels (40). Second, it might be plausible that the aggregations of the TOAC-1, TOAC-8, and TOAC-16 containing Glu(OMe)[7,18,19] analogs observed by cooling from above to below the transition temperature of the lipid would be conserved during the freezing procedure of the samples to 77K. Thirdly, evidence of a tetramer acting as a functional channel was supported by a covalently linked tetramer of alamethicin, the peptide chains of which were linked at the C-termini (74). Finally, tetramer channels were reported for the micelle-associated, peptide venom toxin melittin (75). At this stage of our research, however, many questions remain to be addressed. To further investigate the self-assembling of the alamethicin molecules in the lipid environment, PELDOR/ESEEM experiments in membranes of different lipid compositions, as well as molecular dynamics

simulations in a lipid environment, are in progress. In any case, we believe that our research has opened new perspectives on the characterization of peptide self-aggregated species in membranes at the nm structural level.

CONCLUSIONS

The PELDOR technique, combined with the availability of a set of synthetic alamethicin analogs with spin-labels at well defined positions, has provided quantitative information about the geometry of the supramolecular assembly of this channel-forming antimicrobial molecule. According to two different methods, the relative small number of peptide molecules forming the aggregate was estimated to be ~4. Distance distributions at the nm scale were obtained for three different positions of the peptide chain. For the label position at residue 16, thus located close to the C-terminus of the aggregated peptide, a relatively sharp interspin distance distribution was seen around 2.3 nm. Interestingly, the distances observed for the labels at positions 1 and 8 show distribution maxima at 2.3, 3.2, and 5.2 nm. The intermolecular PELDOR distance of 2.3 nm, independent of the label position, is most likely related to a parallel alignment of the helical molecules. The intramolecular distances between the TOAC-1 and TOAC-16 labels calculated from the molecular model, which was based on the intermolecular PELDOR distances, were found in agreement, within experimental error, with the intramolecular PELDOR distances. The water accessibility of the different spin-label positions qualitatively estimated by the ESEEM experiments was found to follow the order TOAC-1 $>>$ TOAC-8 $\approx$ TOAC-16. This information, along with the PELDOR and molecular modeling data, might support a model, wherein the C-ends of the aggregated peptide molecules are important to stabilize the aggregate, whereas the membrane topology of the N-terminal segments is less well defined. In conclusion, we have shown that the combination of PELDOR, ESEEM, and molecular modeling represents an important tool to investigate the supramolecular structure of a self-assembled spin-labeled peptide aggregate in the lipid membrane-bound state.

We are grateful to Dr. Marco Crisma for providing the coordinates of the x-ray diffraction structure of [TOAC^{16}, Glu(OMe)^{7,18,19}] alamethicin.

This work was supported by the Russian Grant for Scientific Schools (551-2008.3), the Russian Foundation for Basic Research (RFBR grant 06-04-48021-a), the Netherlands Organization of Scientific Research (NWO/RFBR 0.47.017.034), and the Italian Ministry of Foreign Affairs.

REFERENCES

1. Leitgeb, B., L. Szekeres, L. Manczinger, C. Vágvölgyi, and L. Kredics. 2007. The history of alamethicin: a review of the most extensively studied peptaibol. *Chem. Biodivers.* 4:1027–1051.
2. Mueller, P., and P. O. Rudin. 1968. Action potentials induced in biomolecular lipid membranes. *Nature.* 217:713–719.
3. Boheim, G. 1974. Statistical analysis of alamethicin in a lipid membrane. *J. Membr. Biol.* 19:277–303.
4. Sansom, M. S. P. 1993. Alamethicin and related peptaibols—model ion channels. *Eur. Biophys. J.* 22:105–124.
5. Baumann, G., and P. Mueller. 1974. A molecular model of membrane excitability. *J. Supramol. Struct.* 2:538–577.
6. Huang, H. W., and Y. Wu. 1991. Lipid-alamethicin interactions influence alamethicin orientation. *Biophys. J.* 60:1079–1087.
7. Boheim, G. W., W. Hanke, and G. Jung. 1983. Alamethicin pore formation: voltage-dependent flip-flop of α-helix dipoles. *Biophys. Struct. Mech.* 9:181–191.
8. Fox, R. O., and F. M. Richards. 1982. A voltage-gated ion channel model inferred from the crystal structure of alamethicin at 1.5 Å resolution. *Nature.* 300:325–330.
9. Hall, J. E., I. Vodyanov, T. M. Balasubramanian, and G. R. Marshall. 1994. Alamethicin, a rich model for channel behavior. *Biophys. J.* 45:233–247.
10. Cascio, M., and B. A. Wallace. 1988. Conformation of alamethicin in phospholipid vesicles: implications for insertion models. *Proteins Struct. Funct. Genet.* 4:889–898.
11. Pispisa, B., L. Stella, C. Mazzuca, and M. Venanzi. 2006. Reviews in Fluorescence. C. D. Geddes and J. R. Lakowicz, editors. Springer, New York.
12. Kropacheva, T. N., and J. Raap. 2007. Enzymatic reaction in a vesicular microreactor: peptaibol-facilitated substrate transport. *Chem. Biodivers.* 4:1388–1394.
13. Dempsey, C. E., and L. J. Handcock. 1996. Hydrogen bond stabilities in membrane-reconstituted alamethicin from amide-resolved hydrogen-exchange measurements. *Biophys. J.* 70:1777–1788.
14. Bechinger, B., D. A. Skladnev, A. Ogrel, X. Li, E. V. Rogozhkina, et al. 2001. ^{15}N and ^{31}P Solid-state NMR investigations on the orientation of zervamicin II and alamethicin in phosphatidylcholine membranes. *Biochemistry.* 40:9428–9437.
15. Bak, M., R. P. Bywater, M. Hohwy, J. K. Thomsen, K. Adelhorst, et al. 2001. Conformation of alamethicin in oriented phospholipid bilayers determined by ^{15}N solid-state nuclear magnetic resonance. *Biophys. J.* 81:1684–1698.
16. Salnikov, E. S., H. Friedrich, X. Li, P. Bertani, S. Reissmann, et al. 2008. Structure and alignment of the membrane-associated peptaibols ampullosporin A and alamethicin by oriented ^{15}N and ^{31}P solid-state NMR spectroscopy. *Biophys. J.* 113:3034–3042.
17. He, K., S. J. Ludtke, H. W. Huang, and D. L. Worcester. 1995. Antimicrobial peptide pores in membranes detected by neutron in-plane scattering. *Biochemistry.* 34:15614–15618.
18. Salnikov, E. S., M. De Zotti, F. Formaggio, X. Li, C. Toniolo, et al. 2009. Alamethicin topology in phospholipid membranes by oriented solid-state NMR and EPR spectroscopies: a comparison. *J. Phys. Chem. B.* 113:3034–3042.
19. Keller, S. L., S. M. Gruner, and K. Garwisch. 1996. Small concentrations of alamethicin induce a cubic phase in bulk phosphatidylethanolamine mixtures. *Biochim. Biophys. Acta.* 1278:241–246.
20. Angelova, A., R. Ionov, M. H. J. Koch, and J. Rapp. 2000. Interaction of the peptide antibiotic alamethicin with bilayer- and non-bilayer-forming lipids: influence of increasing alamethicin concentration on the lipid supramolecular structures. *Arch. Biochem. Biophys.* 378: 93–106.
21. Spaar, A., C. Münster, and T. Salditt. 2004. Conformation of peptides in membranes studied by X-ray grazing incidence scattering. *Biophys. J.* 87:396–407.
22. Li, C., and T. Salditt. 2006. Structure of magainin and alamethicin in model membranes studied by X-ray reflectivity. *Biophys. J.* 91: 3285–3300.
23. Constantin, D., G. Brotons, A. Jarre, C. Li, and T. Salditt. 2007. Interaction of alamethicin pores in DMPC bilayers. *Biophys. J.* 92: 3978–3987.
24. Qian, S., W. Wang, L. Yang, and H. W. Huang. 2008. Structure of the alamethicin pore reconstructed by X-ray diffraction analysis. *Biophys. J.* 94:3512–3522.

25. Archer, S. J., J. F. Ellena, and D. S. Cafiso. 1991. Dynamics and aggregation of the peptide ion channel alamethicin. *Biophys. J.* 60:389–398.

26. Marsh, D., M. Jost, C. Peggion, and C. Toniolo. 2007. TOAC spin-labels in the backbone of alamethicin: EPR studies in lipid membranes. *Biophys. J.* 92:473–481.

27. Marsh, D., M. Jost, C. Peggion, and C. Toniolo. 2007. Lipid chain length dependence for incorporation of alamethicin in membranes: EPR studies on TOAC-spin-labeled analogues. *Biophys. J.* 92:4002–4011.

28. Bartucci, R., R. Guzzi, M. De Zotti, C. Toniolo, L. Sportelli, et al. 2008. Backbone dynamics of alamethicin bound to lipid membranes: spin-echo electron paramagnetic resonance of TOAC-spin-labels. *Biophys. J.* 94:2698–2705.

29. Milov, A. D., Yu. D. Tsvetkov, F. Formaggio, M. Crisma, C. Toniolo, et al. 2001. The secondary structure of a membrane-modifying peptide in a supramolecular assembly studied by PELDOR and CW-ESR spectroscopies. *J. Am. Chem. Soc.* 123:3784–3789.

30. Milov, A. D., Yu. D. Tsvetkov, E. Y. Gorbunova, L. G. Mustaeva, T. V. Ovchinnikova, et al. 2007. Solvent effects on the secondary structure of the membrane-active zervamicin determined by PELDOR spectroscopy. *Chem. Biodivers.* 4:1243–1255.

31. Milov, A. D., R. I. Samoilova, Yu. D. Tsvetkov, M. De Zotti, C. Toniolo, et al. 2008. PELDOR conformational analysis of bis-labeled alamethicin aggregated in phospholipid vesicles. *J. Phys. Chem. B.* 112: 13469–13472.

32. Milov, A. D., Yu. D. Tsvetkov, F. Formaggio, M. Crisma, C. Toniolo, et al. 2000. Self-assembling properties of membrane-modifying peptides studied by PELDOR and CW-ESR spectroscopies. *J. Am. Chem. Soc.* 122:3843–3848.

33. Milov, A. D., M. I. Samoilova, Yu. D. Tsvetkov, M. Jost, C. Peggion, et al. 2007. Supramolecular structure of self-assembling alamethicin analog studied by ESR and PELDOR. *Chem. Biodivers.* 4:1275–1298.

34. Milov, A. D., R. I. Samoilova, Yu. D. Tsvetkov, F. Formaggio, C. Toniolo, et al. 2007. Self-aggregation of spin-labeled alamethicin in ePC vesicles studied by pulsed electron-electron double resonance. *J. Am. Chem. Soc.* 129:9260–9261.

35. Toniolo, C. 1989. Structure of conformationally constrained peptides: from model compounds to bioactive peptides. *Biopolymers.* 28: 247–257.

36. Toniolo, C., M. Crisma, F. Formaggio, and C. Peggion. 2001. Control of peptide conformation by the Thorpe-Ingold effect (Cα-tetrasubstitution). *Biopolymers.* 60:396–419.

37. Toniolo, C., M. Crisma, and F. Formaggio. 1998. TOAC, a nitroxide spin-labeled, achiral, Cα-tetrasubstituted α-amino acid, is an excellent tool in materials science and biochemistry. *Biopolymers.* 47:153–158.

38. Peggion, C., M. Jost, W. M. de Borggraeve, M. Crisma, F. Formaggio, et al. 2007. Conformational analysis of TOAC-labeled alamethicin F50/5 analogues. *Chem. Biodivers.* 4:1256–1274.

39. Crisma, M., C. Peggion, C. Baldini, E. J. MacLean, N. Vedovato, et al. 2007. Crystal structure of a spin-labeled, channel-forming, alamethicin analogue. *Angew. Chem. Int. Ed.* 46:2047–2050.

40. Vedovato, N., C. Baldini, C. Toniolo, and G. Rispoli. 2007. Pore-forming properties of alamethicin F50/5 inserted in a biological membrane. *Chem. Biodivers.* 4:1338–1346.

41. Woolley, G. A., and B. A. Wallace. 1993. Temperature dependence of the interaction of alamethicin helices in membranes. *Biochemistry.* 32:9819–9825.

42. Milov, A. D., K. M. Salikhov, and M. D. Shirov. 1981. Application of ELDOR in electron-spin echo for paramagnetic center space distribution in solids. *Fiz. Tverd. Tela.* 23:975–982.

43. Milov, A. D., A. G. Maryasov, and Yu. D. Tsvetkov. 1998. Pulsed electron double resonance (PELDOR) and its applications in free-radicals research. *Appl. Magn. Reson.* 15:107–143.

44. Jeschke, G., A. Koch, U. Jonas, and A. Godt. 2002. Direct conversion of EPR dipolar time evolution data to distance distributions. *J. Magn. Reson.* 155:72–82.

45. Milov, A. D., Yu. D. Tsvetkov, F. Formaggio, S. Oancea, C. Toniolo, et al. 2003. Aggregation of spin-labeled trichogin GA IV dimers: distance distribution between spin-labels in frozen solutions by PELDOR data. *J. Phys. Chem. B.* 107:13719–13727.

46. Jeschke, G., G. Panek, A. Godt, A. Bender, and H. Paulsen. 2004. Data analysis procedures for pulse ELDOR measurements of broad distance distributions. *Appl. Magn. Reson.* 26:223–244.

47. Bowman, M. K., A. G. Maryasov, N. Kim, and V. J. DeRose. 2004. Visualization of distance distribution from pulsed double electron-electron resonance data. *Appl. Magn. Reson.* 26:23–40.

48. Milov, A. D., B. D. Naumov, and Yu. D. Tsvetkov. 2004. The effect of microwave pulse duration on the distance distribution function between spin-labels obtained by PELDOR data analysis. *Appl. Magn. Reson.* 26:587–599.

49. Chiang, Y. W., P. P. Borbat, and J. H. Freed. 2005. The determination of pair distributions by pulsed ESR using Tikhonov regularization. *J. Magn. Reson.* 172:279–295.

50. Bode, B. E., D. Margraf, J. Plackmeyer, G. Dürner, T. F. Prisner, et al. 2007. Counting the monomers in nanometer-sized oligomers by pulsed electron-electron double resonance. *J. Am. Chem. Soc.* 129:6736–6745.

51. Dikanov, S. A., and Yu. D. Tsvetkov. 1992. Electron Spin Echo Envelope Modulation (ESEEM) Spectroscopy. CRC Press, Boca Raton, FL.

52. Salnikov, E. S., D. A. Erilov, A. D. Milov, Yu. D. Tsvetkov, C. Peggion, et al. 2006. Location and aggregation of the spin-labeled peptide trichogin GA IV in a phospholipid membrane as revealed by pulsed EPR. *Biophys. J.* 91:1532–1540.

53. Marsh, D. 2001. Polarity and permeation profiles in lipid membranes. *Proc. Natl. Acad. Sci. USA.* 98:777–782.

54. Bartucci, R., R. Guzzi, D. Marsh, and L. Sportelli. 2003. Intramembrane polarity by electron spin echo spectroscopy of labeled lipids. *Biophys. J.* 84:1025–1030.

55. Erilov, D. A., R. Bartucci, R. Guzzi, A. A. Shubin, A. G. Maryasov, et al. 2005. Water concentration profiles in membranes measured by ESEEM of spin-labeled lipids. *J. Phys. Chem. B.* 109:12003–12013.

56. Peggion, C., M. Jost, C. Baldini, F. Formaggio, and C. Toniolo. 2007. Total synthesis in solution of TOAC-labeled alamethicin F50/5 analogues. *Chem. Biodivers.* 4:1183–1199.

57. Szoka, Jr., F., and D. Papahadjopoulos. 1980. Comparative properties and methods of preparation of lipid vesicles (liposomes). *Annu. Rev. Biophys. Bioeng.* 9:467–508.

58. Bartucci, R., D. A. Erilov, R. Guzzi, L. Sportelli, S. A. Dzuba, et al. 2006. Time-resolved electron spin resonance studies of spin-labeled lipids in membranes. *Chem. Phys. Lipids.* 141:142–157.

59. Jorgensen, W. L., D. S. Maxwell, and J. Tirado-Rives. 1996. Development and testing of the OPLS all-atom force field on conformational energetics and properties of organic liquids. *J. Am. Chem. Soc.* 117:11225–11236.

60. Maxwell, D. S., J. Tirado-Rives, and W. L. Jorgensen. 1995. A comprehensive study of the rotational energy profiles of organic systems by ab initio MO theory, forming a base for peptide torsional parameters. *J. Comput. Chem.* 16:984–1010.

61. Parsegian, V. A., N. Fuller, and R. P. Rand. 1979. Measured work of deformation and repulsion of lecithin bilayers. *Proc. Natl. Acad. Sci. USA.* 76:2750–2754.

62. Murzyn, K., T. Róg, W. Blicharski, M. Dutka, J. Pyka, et al. 2006. Influence of the disulfide bond configuration on the dynamics of the spin-label attached to cytochrome *c*. *Proteins.* 62:1088–1100.

63. Rinia, H. A., R. A. Kik, R. A. Demel, M. M. E. Snel, J. A. Killian, et al. 2000. Visualization of highly ordered striated domains induced by transmembrane peptides in supported phosphatidylcholine bilayers. *Biochemistry.* 39:5852–5858.

64. Eaton, S. S., and G. R. Eaton. 2000. Biological Magnetic Resonance, Vol. 19 L. J. Berliner, S. S. Eaton, and G. R. Eaton, editors. Kluwer, New York.

65. Maryasov, A. G., and Yu. D. Tsvetkov. 2000. Formation of the pulsed electron-electron double resonance signal in the case of a finite amplitude of microwave fields. *Appl. Magn. Reson.* 18:583–605.

66. Tikhonov, A. N. 1995. Numerical Methods for the Solution of Ill-Posed Problems. Dordrecht, The Netherlands.

67. Tieleman, D. P., B. Hess, and M. S. P. Sansom. 1998. Analysis and evaluation of channel models. *Biophys. J.* 83:2393–2407.

68. North, C. L., M. Barranger-Mathays, and D. S. Cafiso. 1995. Membrane orientation of the N-terminal segment of alamethicin determined by solid-state ^{15}N NMR. *Biophys. J.* 69:2392–2397.

69. Chen, F.-Y., M.-T. Lee, and H. W. Huang. 2003. Sigmoidal concentration dependence of antimicrobial peptide activities: a case study on alamethicin. *Biophys. J.* 84:3751–3758.

70. Stella, L., M. Burattini, C. Mazzuca, A. Palleschi, M. Venanzi, et al. 2007. Alamethicin interaction with lipid membranes: a spectroscopic study on synthetic analogues. *Chem. Biodivers.* 4:1299–1312.

71. Parker, M. W., J. P. M. Postma, F. Pattus, A. D. Tucker, and D. Tsernoglou. 1992. Refined structure of the pore-forming domain of colicin A at 2.4 Å resolution. *J. Mol. Biol.* 224:639–657.

72. Lakey, J. H., D. Duché, J.-M. González-Manas, D. Baty, and F. Pattus. 1993. Fluorescence energy transfer distance measurements. The hydrophobic helical hairpin of colicin A in the membrane bound state. *J. Mol. Biol.* 230:1055–1067.

73. Savitsky, A., M. Kühn, D. Duché, K. Möbius, and H.-J. Steinhoff. 2004. Spontaneous refolding of the pore-forming colicin A toxin upon membrane association as studied by X-band and W-band high-field EPR spectroscopy. *J. Phys. Chem. B.* 108:9541–9548.

74. Futaki, S., M. Fukuda, M. Omote, K. Yamauchi, T. Yagami, et al. 2001. Alamethicin-leucine zipper hybrid peptide: a prototype for the design of artificial receptors and ion channels. *J. Am. Chem. Soc.* 123:12127–12134.

75. Brown, L. R., J. Jauterwein, and K. Wüthrich. 1980. High-resolution ^{1}H-NMR studies of self-aggregation of melittin in aqueous solution. *Biochim. Biophys. Acta.* 622:231–244.